



First-principles investigation of electronic and optical properties and thermodynamic stability of $Zn_{1-x}Be_xO$ semiconductor alloy



Said Lakel^{a,b,*}, Fatima Elhamra^a, K. Almi^c, H. Meradji^d

^a Laboratory of Physical Materials – University of LAGHOUAT, BP 37G, Laghouat, Algeria

^b Laboratoire de Matériaux Semi Conducteurs et Métalliques, Université de Biskra, Algeria

^c Laboratoire de Génie Energétique et Matériaux, LGEM, Université de Biskra, Algeria

^d Laboratoire de Physique des Rayonnements, Université Badji Mokhtar Annaba, Algeria

ARTICLE INFO

Article history:

Received 10 June 2015

Received in revised form

21 July 2015

Accepted 22 July 2015

Keywords:

DFT

$Zn_{1-x}Be_xO$

Electronic properties

Optic properties

Thermodynamic properties

ABSTRACT

The electronic, optical and thermodynamic properties of beryllium doped zinc oxide ($Zn_{1-x}Be_xO$) ternary mixed crystal are studied by the first-principle calculations within the framework of the density functional theory (DFT). Our calculated lattice constants for ZnO and BeO are in good agreement with the available theoretical and experimental data. The lattice constants decrease with Be concentration increasing. The calculated band structure shows that all considered compounds are direct gap semiconductors. The density of states and optical constants such as complex dielectric function, extinction coefficient, refractive index and absorption coefficient are also calculated and analyzed in detail. Moreover, the thermodynamic stability of these alloys is investigated by the calculated $T-x$ phase diagram.

© 2015 Elsevier Ltd. All rights reserved.

1. Introduction

The semiconductor ZnO has gained substantial research interests as a satisfactory material in optoelectronic applications due to its wide band gap (3.37 eV) and large exciton binding energy (60 mV) [1,3]. It is commonly believed that one of the crucial steps in designing modern optoelectronic devices is the modulation of band gap, which could be realized through the addition of a metal element (e.g., Mg or Cd) in ZnO [2,5]. The doping effects of Mg and Cd, however, are limited and unreliable due to the low solubility of Mg and Cd in ZnO, as well as the different crystal structures and large lattice mismatch between MgO (CdO) and ZnO [4,5].

Band-gap engineering of ZnO can be achieved by alloying with MgO ($E_g=7.70$ eV) for UV applications and such alloy can also be used as barrier layers in ZnO/(Zn,Mg)O superlattices for quantum well devices [6,7]. However, the phase separation occurs in $Zn_{1-x}Mg_xO$ solid solutions when the Mg composition exceeds 33% [7]. This is due to the differences in the crystal structures of ZnO [wurtzite, $P63mc$] and MgO (cubic, rocksalt). As such, the UV absorption range is limited to 3.37–3.90 eV in the $Zn_{1-x}Mg_xO$ system for $x < 0.33$ [8].

On the other hand, the element Be is widely regarded as a promising candidate to tune the band gap of ZnO, due to the following considerations [4,5,9]. First, BeO and ZnO have the same stable structure of hexagonal wurtzite [4]. Second, the solubility of Be in ZnO can vary over the entire composition range from 0% to 100%, and there is no phase segregation between BeO and ZnO [4]. Third, BeO has a big band gap of 10.6 eV, allowing the modulation of band gap in a wide range from 3.4 to 10.6 eV [4]. Forth, the $Zn_{1-x}Be_xO$ alloy can be easily synthesized by mixing ZnO with Be [9]. Furthermore, as the band gap in $Zn_{1-x}Be_xO$ can theoretically be tuned from 3.37 to 10.60 eV, this materials system may replace $Zn_{1-x}Mg_xO$ solid solutions which are being considered in applications such as polymer-oxide hybrid solar cells, field effect transistors, high- k films on Si, quantum Hall effect devices, acoustic resonators and large electromechanical coupling [10–13].

In this work, we mix ZnO with BeO in the wurtzite structure and perform a theoretical study of the structural, electronic, optical and thermodynamic properties of $Zn_{1-x}Be_xO$ alloys ($x=0, 0.25, 0.50, 0.75$ and 1.0) using plane-wave pseudopotential method. The optical properties are investigated in detail for $Zn_{1-x}Be_xO$ alloys. The results obtained are in good agreement with the available experimental data and other theoretical calculation. In Section 2, a brief description of computational method is given. The results of optical properties are discussed in Section 3. The

* Correspondence to: Laboratory of Metallic and Semiconducting Materials, University of Biskra, B.P.145, Biskra, Algeria. Tel: +7 71 40 94 03.

E-mail address: s.lakel@yahoo.fr (S. Lakel).

results obtained are also compared with other available theoretical results and existing experimental data. Finally, the summary of our main results and conclusion are given in Section 4.

2. Computational details

Our calculations are performed using the plane-wave pseudo potential method based on density functional theory [14] as implemented in the CASTEP codes [15]. The exchange and correlation potential is treated within the generalized gradient approximation (GGA) in the Perdew–Burke–Eruzerhof scheme [16]. The valence electron configurations are taken as $3d^{10}4s^2$ for Zn, $2s^22p^4$ for O and $2s^2$ for Be, respectively, to describe the electron-ion interaction. Fig. 1 shows the structure of the 16-atom supercell used in the present study, which corresponds to $2 \times 2 \times 1$ of the conventional wurtzite cell. The numbered atoms are Zn or Be, and the dark atoms are O. According to the special quasi random structures (SQS) approach [17], the $Zn_{1-x}Be_xO$ ($x=0, 0.25, 0.5, 0.75, 1.0$) structures can be obtained by replacing 1 to 8 Zn atoms with Be in the $2 \times 2 \times 1$ wurtzite ZnO supercell (see Fig. 1). The electronic wave functions are expanded in plane wave basis set with the cutoff energy of 700 eV. The integration over the Brillouin zone is performed using the Monkhorst–Pack method [18] with a separation of $0.021/\text{\AA}$ for all compounds. The tolerances for geometry optimization are set as follows: The difference of the total energy is within 1×10^{-6} eV/atom, the maximum force is 0.01 eV/Å, the maximum stress is 0.02 GPa and the maximum displacement is 5.0×10^{-4} Å.

In addition, to investigate electronic and optical properties accurately, more k -points are needed and a denser $8 \times 8 \times 10$ k -points are generated. Furthermore, the number of conduction bands is also an important parameter in the calculation, which defines the energy range covered and determines the accuracy of the Kramers–Kronig transform. In present work, 20 empty bands in addition to the occupied bands are included.

3. Results and discussions

3.1. Structural properties

The structural properties of the binary compounds ZnO and BeO and their ternary alloys $Zn_{1-x}Be_xO$ with three special compositions $x=0.25, 0.50$ and 0.75 are investigated in the wurtzite structure. The calculated lattice constants and bulk modulus are listed in Table 1, along with the available data. It can be clearly seen that our calculated results are in good agreement with the experimental and theoretical data [19,22]. The calculated lattice constants parameters of $Zn_{0.75}Be_{0.25}O$, $Zn_{0.5}Be_{0.5}O$ and $Zn_{0.25}Be_{0.75}O$ are in agreement with theoretical work [21]. The

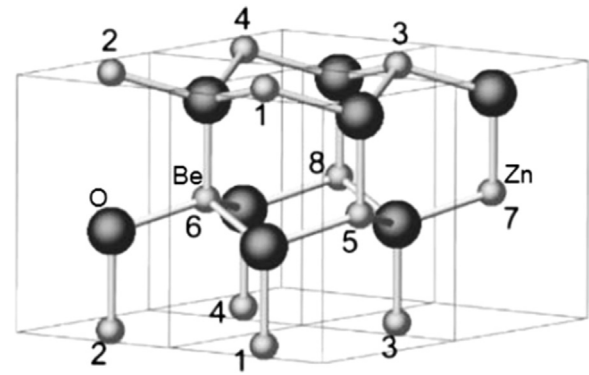


Fig. 1. The 16-atom supercell of a wurtzite structure. Eight cation sites are labeled.

results listed in Table 1 show that the lattice constants, a and c , decrease with increasing Be concentration. This phenomenon occurs because the atom radius of beryllium is smaller than that of zinc.

Mainly, due to the experimental data being rare, it is assumed that the atoms are located at the ideal lattice sites and the lattice constant varies linearly with composition x according to Vegard's law [23]

$$P(A_{1-x}B_xC) = x P_{BC} + (1-x)P_{AC}; \quad P = a \text{ or } c \quad (1)$$

where $P_{BC}(a_{BC}$ or $c_{BC})$ and $P_{AC}(a_{AC}$ or $c_{AC})$ are the equilibrium lattice constants of the binary compounds BC and AC, respectively, $P(A_{1-x}B_xC)$ is the alloy lattice constants.

Hence, the lattice constant can be written as:

$$P(A_{1-x}B_xC) = x P_{BC} + (1-x)P_{AC} - x(1-x)b; \quad P = a \text{ or } c \quad (2)$$

where the quadratic term b is the bowing parameter.

It is found that the deviation of the optimized lattice constants from linearity is relatively small. Due to the small mismatching between the lattice constants of ZnO and BeO, the small bowing parameter b is calculated to be 0.028 Å and 0.178 Å for a and c , respectively. Moreover, since the ionic radius of Be^{2+} is smaller than that of Zn^{2+} , the lattice constants a and c decrease with increasing Be concentration. This causes the material to be more rigid, and therefore it increases the bulk modulus of $Zn_{1-x}Be_xO$ alloys.

3.2. Electronic properties

The calculated band structures along the high symmetry directions of the $Zn_{1-x}Be_xO$ alloys with different concentration x are shown in Fig. 2. For ZnO, the maximum of the valence band and the minimum of the conduction band locates at G point, showing it is a direct band gap semiconductor. It is obvious that other

Table 1

Calculated lattice constants a and c of $Zn_{1-x}Be_xO$ after geometric optimization compared with available theoretical and experimental data.

	x	a (Å)			c (Å)		
		This work	Expt.	Other calculations	This work	Expt.	Other calculations
$Zn_{1-x}Be_xO$	0	3.275	3.258 ^a	3.283 ^b , 3.256 ^c	5.304	5.220 ^a	5.309 ^b , 5.256 ^c
	0.25	3.145		3.134 ^c	5.132		5.076 ^c
	0.5	2.915		2.972 ^c	4.970		4.99 ^c
	0.75	2.788		2.889 ^c	4.528		4.675 ^c
	1	2.714	2.698 ^d	2.764 ^c	4.412	4.377 ^d	4.487 ^c

^a Ref. [19].

^b Ref. [20].

^c Ref. [21].

^d Ref. [22].

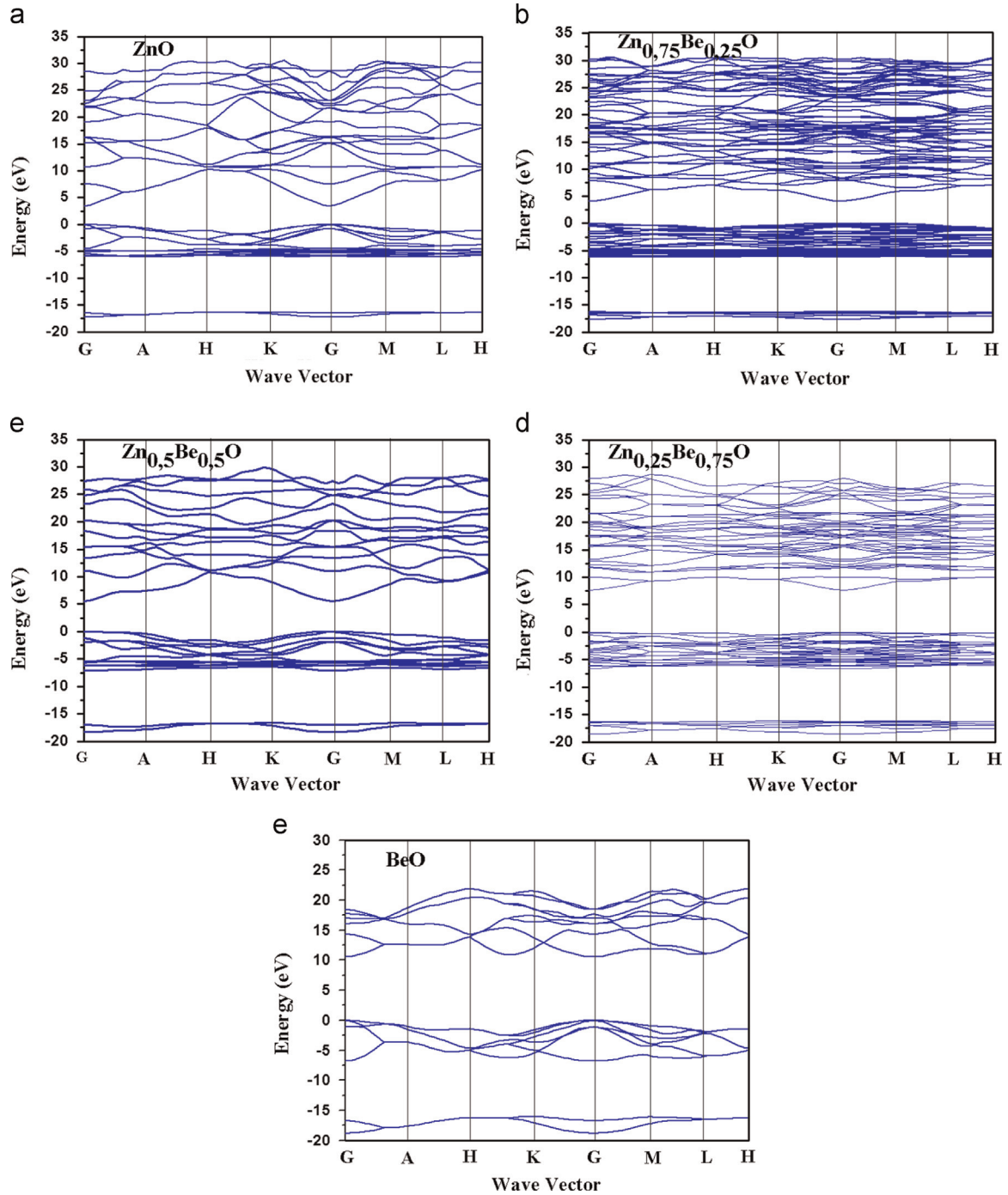


Fig. 2. Calculated band structure of ZnO (a), BeO (e), $Zn_{0.75}Be_{0.25}O$ (b), $Zn_{0.5}Be_{0.5}O$ (c) and $Zn_{0.25}Be_{0.75}O$ (d).

$Zn_{1-x}Be_xO$ ($x=0.25, 0.50, 0.75, 1$) alloys also exhibit a direct band gap (G–G) character. Moreover, the band gap of all $Zn_{1-x}Be_xO$ shows an increasing feature varying with the molar fraction x .

It is shown in Table 2 that the calculated band gap for ZnO is in accordance with the previous theoretical results [24,26], but is smaller than the experimental value of 3.37 eV [25]. The underestimation of the calculated band gap is a common phenomenon for both LDA and GGA, which is attributed to the self-interaction error and the absence of derivative discontinuity in the exchange–correlation potential [27,28]. But this will not affect the analysis of the electronic structure. From Table 2, we also note that the band gap energy increases with x increasing, which is due to the fact that the conduction bands shift to high energy. In order to close to

the experimental value, Band gap value has been corrected, using the formula

$$E_{g,Zn_{1-x}Be_xO}^{cor} = E_{g,Zn_{1-x}Be_xO}^{cal} + (1-x)\Delta E_{ZnO} + x\Delta E_{BeO} \quad (3)$$

$E_{g,Zn_{1-x}Be_xO}^{cor}$ is correction band gap of $Zn_{1-x}Be_xO$, $E_{g,Zn_{1-x}Be_xO}^{cal}$ is calculation band gap of $Zn_{1-x}Be_xO$, x is concentration of Be, ΔE_{ZnO} is experimental band gap minus calculated band gap of ZnO, ΔE_{BeO} is experimental band gap minus calculated band gap of BeO. Correction parameters are experimental of ZnO 3.32 eV and experimental of BeO 10.6 eV, Table 2 shown our calculated compared with experimental and our calculated results are consistent with experimental results.

Fig. 3(a) and (b) show the partial densities of states of ZnO and

Table 2
Calculated band gap energy for $Zn_{1-x}Be_xO$ alloys.

x		0	0.25	0.5	0.75	1
E_g (eV)	This work	0.982	1.874	4.751	5.55	7.67
	Theoretical	0.971 ^a	1.805 ^a	4.702 ^a	5.463 ^a	7.320 ^a
	Correctional	3.32	4.40	5.55	7.53	10.60
	Experimental	3.37 ^b				10.585 ^b

^a Ref. [24].

^b Ref. [25].

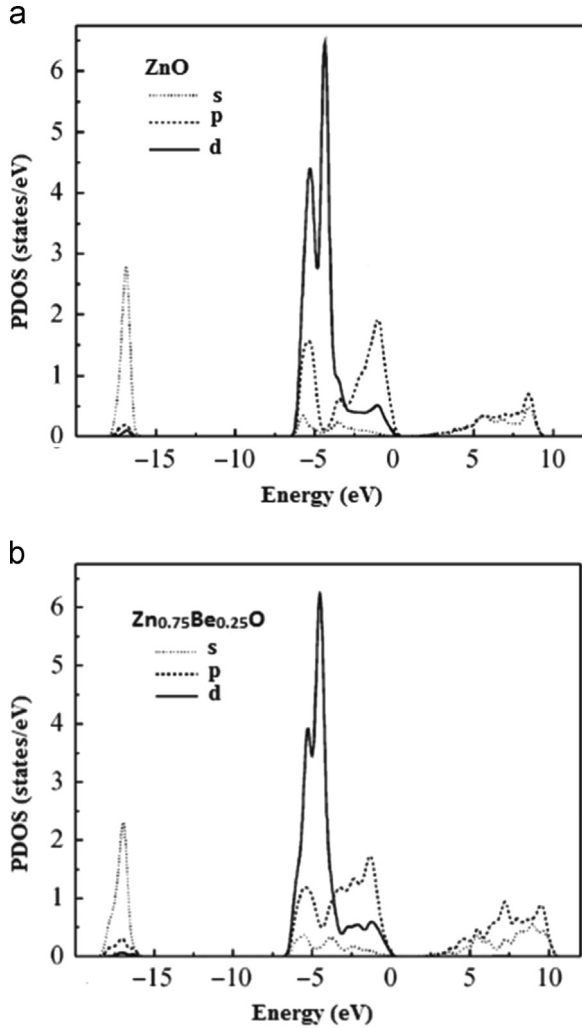


Fig. 3. Partial density of states for (a) ZnO (b) and $Zn_{0.75}Be_{0.25}O$.

$Zn_{0.75}Be_{0.25}O$, respectively. From the figures, it is found that the valence band consists mainly of O (2s), (O2p) and Zn (3d) orbital's. The O (2s) orbital's are located around -17.1 eV with a band range of about 0.66 eV, indicating that these states have been strongly confined and cannot interact with others. The O (2s) orbital's are predominantly found between -3.15 and 0.18 eV in the uppermost valence band while the Zn (3d) orbital's with two peaks appear in the range from -6.55 to -3.10 eV. The electron transition between Zn (3d) and O (2p) orbitals leads to slight movement of O partial state density to lower energy band, indicating that ZnO is a metal oxide semi-conductor. With the Be doping, the position of O(2s) orbitals does not change evidently but its band rang increases slightly to 0.75 eV. Although the Zn (3d) and O (2p)

orbital's are all located in the valence band, the uppermost valence band are dominated by O (2p) orbital's. So; the valence band maximum (VBM) of $Zn_{1-x}Be_xO$ alloys is mainly determined by O (2p) orbital's. Moreover, the conduction band is mainly formed by Zn (4s); Zn (3p) and Be (2s).

Now, we further investigate the change of the band by analyzing the partial density of states (PDOS) in different compositions x . Fig. 4 shows the state densities of O (2p), Zn (4s), Zn (3p) and Be (2s). This figure shows that, the uppermost valence bands of O (2p) orbital's do not change obviously; in the conduction band, the Be (2s) orbital's are enhanced with the increasing composition x and the positions of peaks for Zn (4s), Zn (3p) and Be (2s) shift toward the higher energy. Moreover, it is clearly observed that the lowest conduction band which determines the conduction band minimum (CBM) is dominated by Zn 4s orbital's. As a result, the Zn (4s) orbital's shift toward the higher energy band and the corresponding band gap is enlarged.

3.3. Optical properties

An understanding of the optical properties of $Zn_{1-x}Be_xO$ alloys is of great importance to their applications in optoelectronic devices. The optical properties can be derived from the complex dielectric function $\epsilon(\omega)$ written as

$$\epsilon(\omega) = \epsilon_1(\omega) + i \epsilon_2(\omega) \quad (4)$$

The imaginary part of the dielectric function $\epsilon_2(\omega)$ is expressed as follows [29]:

$$\epsilon_2(\omega) = \frac{4\pi e^2}{\Omega \epsilon_0} \sum_{K,V,C} |\phi_K^C \langle u, r | \phi_K^V \rangle|^2 \delta(E_K^C - E_K^V - \omega) \quad (5)$$

where e is the electric charge, Ω is the unit cell volume, u is the vector defining the polarization of the incident electric field, ω is the frequency of the light, ϕ_K^C and ϕ_K^V are the wave functions of the conduction and valence bands, respectively. The real part of the dielectric function can be evaluated from $\epsilon_2(\omega)$ using the Kramers–Kronig relations [30]:

$$\epsilon_1(\omega) = 1 + \frac{2P}{\pi} \int_0^\infty \frac{\omega' \epsilon_2(\omega')}{\omega'^2 - \omega^2} d\omega' \quad (6)$$

With the knowledge of the complex dielectric function, other optical constants such as refractive index $n(\omega)$, extinction coefficient $k(\omega)$ and absorption coefficient $\alpha(\omega)$ can be calculated using the formulas as follows [31–33]:

$$n(\omega) = \frac{1}{\sqrt{2}} \left[(\epsilon_1^2 + \epsilon_2^2)^{1/2} + \epsilon_1 \right]^{1/2} \quad (7)$$

$$k(\omega) = \frac{1}{\sqrt{2}} \left[(\epsilon_1^2 + \epsilon_2^2)^{1/2} - \epsilon_1 \right]^{1/2} \quad (8)$$

$$\alpha(\omega) = \sqrt{2} \omega \left[\sqrt{(\epsilon_1^2 + \epsilon_2^2)} - \epsilon_1 \right]^{1/2} \quad (9)$$

Fig. 5 illustrates the imaginary part of the dielectric function of $Zn_{1-x}Be_xO$ alloys with different composition x . Our analysis of $\epsilon_2(\omega)$ curve shows that the first critical point of the dielectric function at $x=0.0, 0.25, 0.50, 0.75, 1.0$ occurs around 3.02 eV, 3.85 eV, 6.1 eV, 7.68 eV and 10.15 eV, along polarization direction (001) and 2.51 eV, 3.05 eV, 4.98 eV, 7.50 eV and 10.14 eV along polarization direction (100), respectively. It is obvious that the critical point shifts towards higher energies with the increase of Be concentration. Moreover, with the increasing Be concentration, the anisotropic behaviors of the $\epsilon_1(\omega)$ in and $\epsilon_2(\omega)$ functions reduce obviously along different polarization directions.

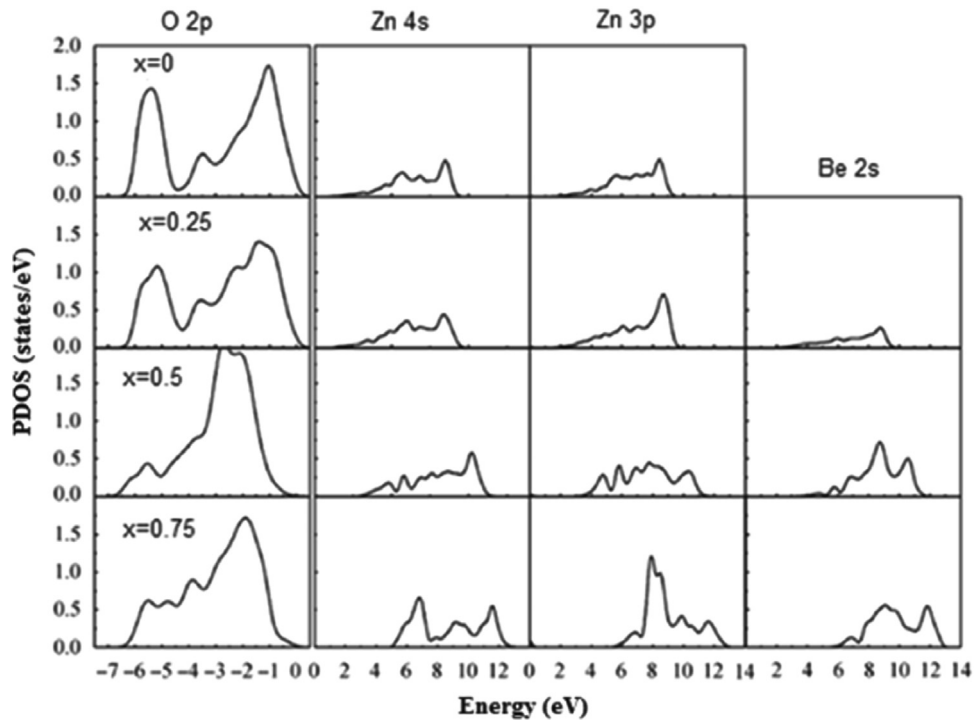


Fig. 4. Valence band of O2p and conduction bands of Zn (4s), Zn (3p) and Be (2s) for $Zn_{1-x}Be_xO$ with different compositions x .

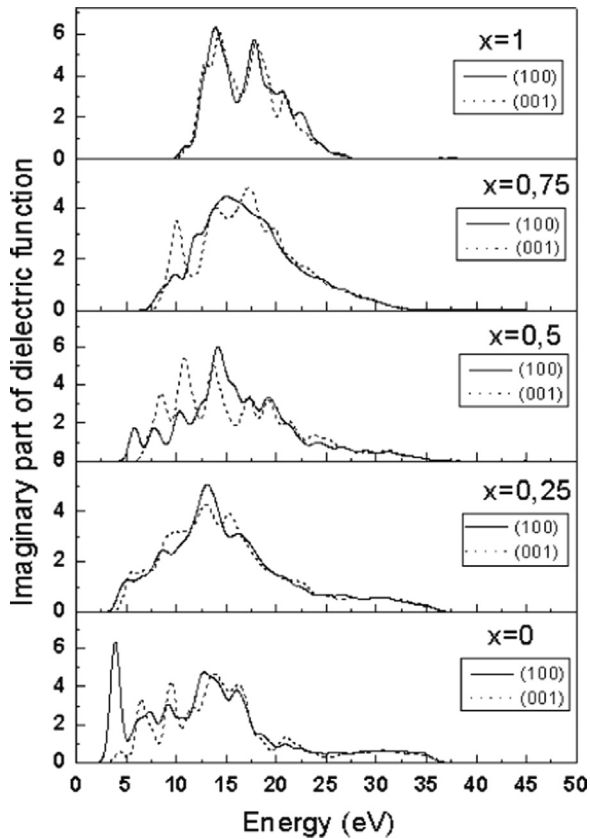


Fig. 5. Calculated imaginary parts of the dielectric function of $Zn_{1-x}Be_xO$ alloys along polarization directions (001) and (100).

The real parts of the dielectric function for the considered compounds are displayed in Fig. 6. It is well known that the zero frequency limits $\epsilon_1(0)$ is an important quantity, which represents the dielectric response to the static electric field. The calculated

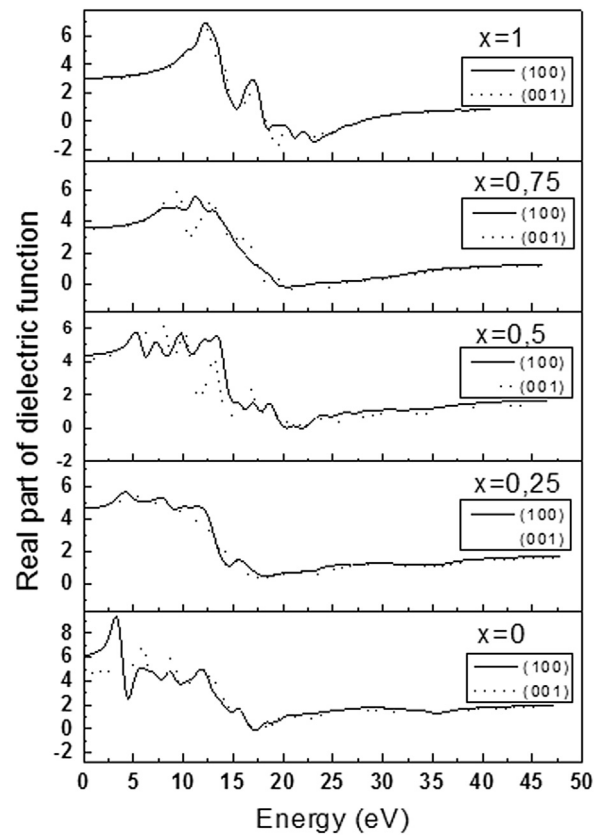


Fig. 6. The real parts of the dielectric function for $Zn_{1-x}Be_xO$ alloys along polarization directions (001) and (100).

static dielectric constants of the $Zn_{1-x}Be_xO$ alloys are listed in Table 3. The static dielectric constants of the $Zn_{1-x}Be_xO$ alloys at considered compositions are 4.64, 4.42, 3.48, 3.3 and 2.98 along polarization direction (001) and 6.18, 4.59, 3.58, 3.35 and 3.02

Table 3
Dielectric constant (ϵ_1) and refractive index (n) for $\text{Zn}_{1-x}\text{Be}_x\text{O}$ alloys.

x Direction	0		0.25		0.5		0.75		1	
	(001)	(100)	(001)	(100)	(001)	(100)	(001)	(100)	(001)	(100)
$\epsilon_1(0)$	4.64	6.18	4.42	4.59	3.48	3.58	3.3	3.35	2.98	3.02
n	5.49 ^a	9.47 ^a							3.02 ^a	3.09 ^a
	2.15	2.48	2.10	2.14	1.84	1.86	1.81	1.79	1.73	1.74
	2.35 ^a								1.73 ^b	

^a Ref.[34],

^b Ref.[35]

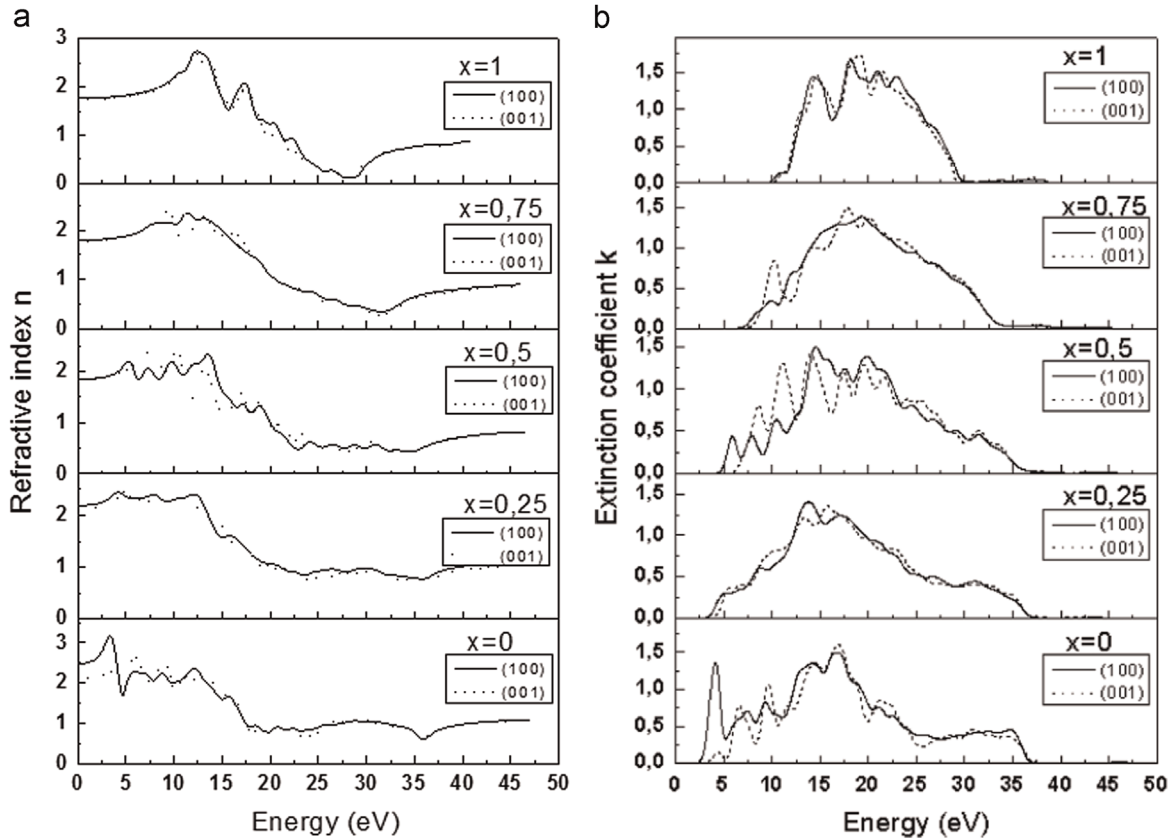


Fig. 7. (a) Refractive index and (b) extinction coefficient for $\text{Zn}_{1-x}\text{Be}_x\text{O}$ corresponding to different values of x .

along polarization direction (100) corresponding to $x=0.0, 0.25, 0.50, 0.75$ and 1.0 , respectively. It indicates that the static dielectric constants reduce with increasing Be concentration. In the range $0.0\text{--}12.0$ eV, as x increases, the first strong peak in $\epsilon_1(\omega)$ shifts towards higher incident photon energy.

The refractive index and the extinction coefficient of $\text{Zn}_{1-x}\text{Be}_x\text{O}$ with different concentration x are presented in Fig. 7. From Fig. 7a, we can see that the static refractive index $n(0)$ for $x=0.0, 0.25, 0.50, 0.75, 1.0$ are found to be $2.15, 2.10, 1.84, 1.81$ and 1.73 along polarization direction (001) and $2.48, 2.14, 1.86, 1.79$ and 1.74 along polarization direction (100) corresponding to $x=0.0, 0.25, 0.50, 0.75$ and 1.0 , respectively, which are in good agreement with the values derived from the real part of the dielectric function (see Table 3). It is also noted that for all considered compounds, the refractive index first increases and then decreases as the energy increases. It is clear from Fig. 7b that the extinction coefficient follows the trend of the imaginary part of the dielectric function.

Fig. 8 shows the absorption coefficients of all the studied

compounds. There is a gradual shift in the absorption edges of the $\text{Zn}_{1-x}\text{Be}_x\text{O}$ alloys with the increase of concentration. Moreover, we also note that the strong absorption region is gradually broadened as x increasing.

3.4. T - x phase diagram

In order to investigate the phase stability of the $\text{Zn}_{1-x}\text{Be}_x\text{O}$ alloys, we calculated the phase diagram based on the regular-solution model [36–38]. The Gibbs free energy of mixing ΔG_m for alloys can be written as:

$$\Delta G_m = \Delta H_m - T\Delta S_m \quad (10)$$

where

$$\Delta H_m = \Omega_m x(1-x) = E_{\text{Zn}_{1-x}\text{Be}_x\text{O}} - xE_{\text{BeO}} - (1-x)E_{\text{ZnO}} \quad (11)$$

$$\Delta S_m = -R[x \ln x + (1-x)\ln(1-x)] \quad (12)$$

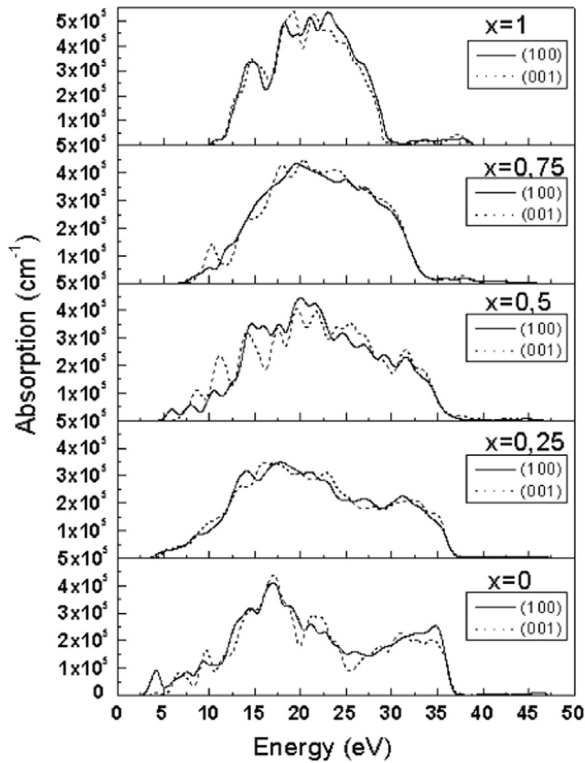


Fig. 8. Absorption coefficient of $Zn_{1-x}Be_xO$ alloys.

ΔH_m and ΔS_m are the enthalpy and entropy of mixing, respectively; Ω is the interaction parameter depending on the material; $E(Zn_{1-x}Be_xO)$, E_{ZnO} and E_{BeO} are the respective energies of the $Zn_{1-x}Be_xO$ alloy and the binary compounds ZnO and BeO; R is the gas constant and T is the absolute temperature. Using Eq. (11), we have obtained Ω as a function of concentration by a linear fit: $\Omega = 10.63x + 11.14$ (kJ/mol). The average of Ω in the range $0 \leq x \leq 1$ is calculated to be 16.445 kJ/mol.

Using Eqs. (10)–(12), we calculated ΔG_m at different concentrations to determine the T - x phase diagram which shows the stable, metastable and unstable mixing regions of the alloys. The calculated phase diagram of the $Zn_{1-x}Be_xO$ alloys is represented in Fig. 9. The binodal curve, which is the stable phase boundary line, can be calculated by the common tangent line touches the ΔG_m curve. The spinodal curve, which indicates the miscibility gap, is determined as those points at which the second derivative of the free energy is zero. The wide range between spinodal and binodal curves suggests that this alloy may exist as a metastable phase. We also observe the critical temperature T_c , which is the lowest temperature the alloys could be formed, indicating the thermodynamic stability of alloys over the entire composition range, equals to 2955 K. The results imply that the $Zn_{1-x}Be_xO$ alloys are stable under high temperature.

4. Conclusions

In this paper, we have used the first-principle calculations to study the lattice parameters, electronic, optical and thermodynamic properties of the $Zn_{1-x}Be_xO$ ternary mixed crystals. The calculated lattice constants agree well with the experimental data and other calculations. The variations of lattice constants as a function of composition are discussed. Our calculated band structure exhibits the direct gap semiconductor nature of $Zn_{1-x}Be_xO$ alloys. After correction the electronic band gap is

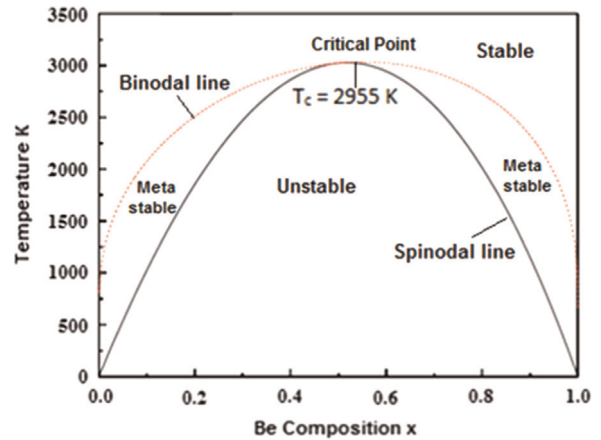


Fig. 9. T - x phase diagram for $Zn_{1-x}Be_xO$ alloy. Solid line: spinodal curve; dot line: binodal line.

consistent with experimental results. Analysis of density of states reveals Zn (4s), Zn (3p) and Be (2s) states are the main conductors. The complex dielectric function, refractive index, extinction coefficient and absorption coefficient are also obtained and analyzed. Finally, the stable, metastable and unstable regions of the alloys are shown by the calculated T - x phase diagram.

References

- [1] J. Sun, H.T. Wang, J. He, Y. Tian, *Phys. Rev. B* 71 (2005) 125132.
- [2] X.F. Fan, Z.X. Shen, Y.M. Lu, Jer-Lai Kuo, *New J. Phys.* 11 (2009) 093008.
- [3] U. Ozgur, Ya.I. Alivov, C. Liu, A. Teke, M.A. Reschikov, S. Dog'an, V. Avrutin, S.-J. Cho, H. Morkoc, *J. Appl. Phys.* 98 (2005) 041301.
- [4] Y.R. Ryu, T.S. Lee, J.A. Lubguban, A.B. Corman, H.W. White, J.H. Leem, M.S. Han, Y.S. Park, C.J. Youn, W.J. Kim, *Phys. Lett.* 88 (2006) 241108.
- [5] W.J. Kim, J.H. Leem, M.S. Han, I.-W. Park, Y.R. Ryu, T.S. Lee, *J. Appl. Phys.* 99 (2006) 096104.
- [6] T. Makino, Y. Segawa, M. Kawasaki, A. Ohtomo, R. Shiroki, K. Tamura, T. Yasuda, H. Koinuma, *Appl. Phys. Lett.* 78 (2001) 1237–1239.
- [7] Y.R. Ryu, T.S. Lee, J.A. Lubguban, A.B. Corman, H.W. White, J.H. Leem, M.S. Han, Y.S. Park, C.J. Youn, W.J. Kim, *Appl. Phys. Lett.* 88 (2006) 052103–052105.
- [8] X.F. Fan, Z. Zhu, Y.S. Ong, Y.M. Lu, Z.X. Shen, J.L. Kuo, *Appl. Phys. Lett.* 91 (2007) 121121–121123.
- [9] J.H. Yu, D.S. Park, J.H. Kim, T.S. Jeong, C.J. Youn, K.J. Hong, *J. Mater. Sci.* 45 (2010) 130–135, *J. Cryst. Growth* 312 (2010) 1683–1686.
- [10] M. Nakano, A. Tsukazaki, A. Ohtomo, K. Ueno, S. Akasaka, H. Yuji, K. Nakahara, T. Fukumura, M. Kawasaki, *Adv. Mater.* 22 (2010) 876–879.
- [11] D.C. Olson, S.E. Shaheen, M.S. White, W.J. Mitchell, M.F.A.M. van Hest, R. T. Collins, D.S. Ginley, *Adv. Funct. Mater.* 17 (2007) 264–269.
- [12] A. Tsukazaki, S. Akasaka, K. Nakahara, Y. Ohno, H. Ohno, D. Maryenko, A. Ohtomo, M. Kawasaki, *Nat. Mater.* 9 (2010) 889–893.
- [13] Y. Chen, P. Reyes, Z. Duan, G. Saraf, R. Wittstruck, Y. Lu, O. Taratula, E. Galoppini, *J. Electron. Mater.* 38 (2009) 1605–1611.
- [14] P. Hohenberg, W. Kohn, *Phys. Rev.* 136 (1964) B864.
- [15] M. Segall, P.J. Lindan, M. Probert, C. Pickard, P. Hasnup, S. Clark, M. Payne, *J. Phys.: Condens. Matter* 14 (2002) 2717.
- [16] J.P. Perdew, K. Burke, M. Ernzerhof, *Phys. Rev. Lett.* 77 (1996) 3865.
- [17] A. Zunger, S.H. Wei, L.G. Ferreira, J.E. Bernard, *Phys. Rev. Lett.* 65 (1990) 353–356.
- [18] H.J. Monkhorst, J.D. Pack, *Phys. Rev. B* 13 (1976) 5188.
- [19] F. Decremps, F. Datchi, A.M. Saitta, A. Polian, S. Pascarelli, A. Di Cicco, J.P. Itié, F. Baudelet, *Phys. Rev. B* 68 (2003) 104101.
- [20] A. Schleife, F. Fuchs, J. Furthmüller, F. Bechstedt, *Phys. Rev. B* 73 (2006) 245212.
- [21] Zheng Yongping, Chen Zhigao, Lu Yu, Wu Qingyun, Weng Zhenzhen, Huang Zhigao, *Chin. J. Semicond.* 29 (12) (2008) 2316–2321.
- [22] R.M. Hazen, L.W. Finger, *J. Appl. Phys.* 59 (1986) 3728.
- [23] L. Vegard, *Z. Phys. A: Hadron. Nucl.* 5 (1921) 17.
- [24] S.F. Ding, G.H. Fan, S.T. Li, K. Chen, B. Xiao, *Phys. B*, 394, (2007) 127–131.
- [25] M. Städele, J.A. Majewski, P. Vogl, A. Görling, *Phys. Rev. Lett.* 79 (1997) 2089.
- [26] B. Baumeier, P. Krüger, J. Pollmann, *Phys. Rev. B* 75 (2007) 045323.
- [27] R. Godby, M. Schlüter, L. Sham, *Phys. Rev. Lett.* 56 (1986) 2415.
- [28] O. Madelung (Ed.), *Semiconductors: Data Handbook*, third ed., Springer, Berlin, 2004.
- [29] A. Delin, P. Ravindran, O. Eriksson, J.M. Wills, *Int. J. Quant. Chem.* 69 (1998) 349–358.
- [30] M. Alouani, J. Wills, *Phys. Rev. B* 54 (1996) 2480.
- [31] M. Dressel, *Electrodynamics of Solids: Optical Properties of Electrons in Matter*, Cambridge University Press, 2002.

- [32] A.M. Fox, *Optical Properties of Solids*, Oxford University Press, 2001.
- [33] S. Saha, T. Sinha, A. Mookerjee, *Phys. Rev. B* 62 (2000) 8828.
- [34] L.Àu Bing, Zhou Xun, Linghu Rong-Feng, Wang Xiao-Lu, Yang Xiang-Dong Chin, *Phys. B* 3 (2011) 036104.
- [35] T.S. Yen, C.K. Kuo, W.L. Han, Y.H. Qui, Y.Z. Huang, *J. Am. Ceram. Soc.* 66 (1983) 860.
- [36] R.A. Swalin, R.A. Swalin, *Thermodynamics of Solids*, J. Wiley, New York, NY, 1972.
- [37] L.G. Ferreira, S.-H. Wei, A. Zunger, *Phys. Rev. B* 40 (1989) 3197.
- [38] L. Teles, J. Furthmüller, L. Scolfaro, J. Leite, F. Bechstedt, *Phys. Rev. B* 62 (2000) 2475.